

Reactivity of Di-Iodine toward Thiol: Desulfuration Reaction of 5-Nitro-2-mercapto-benzimidazole upon Reaction with Di-Iodine

G. J. Corban,¹ C. D. Antoniadis,¹ S. K. Hadjikakou,¹
N. Kourkoumelis,² V. Yu. Tyurin,³ A. Dolgano,⁴ E. R. Milaeva,³
M. Kubicki,⁵ P. V. Bernhardt,⁶ E. R. T. Tiekink,⁷ S. Skoulika,⁸
and N. Hadjiliadis¹

¹Section of Inorganic and Analytical Chemistry, Department of Chemistry, University of Ioannina, 45110 Ioannina, Greece

²Medical Physics Laboratory, Medical School, University of Ioannina, 45110 Ioannina, Greece

³Department of Chemistry, M. V. Lomonosov Moscow State University, 119991 Moscow, Russian Federation

⁴Institute of Organoelement Compounds of Russian Academy of Sciences, 119992 Moscow, Russian Federation

⁵Department of Chemistry, A. Mickiewicz University, 60-780 Poznań, Poland

⁶Department of Chemistry, The University of Texas, San Antonio, TX 78249-0698, USA

⁷School of Molecular and Microbial Sciences, University of Queensland, Brisbane 4072, Australia

⁸Section of Physical Chemistry, Department of Chemistry, University of Ioannina, 45110 Ioannina, Greece

Received 2 March 2012

ABSTRACT: The reaction of 2-mercapto-benzoic acid (H_2MBA), 2-mercapto-nicotinic acid (H_2MNA), and 2-mercapto-pyrimidine (PMT) with a twofold molar amount of di-iodine (I_2) results in the isolation of crystals of the neutral disulfides of formulae: $\{(HMBA)_2 \cdot 1/2(CH_3CN)\}$ (**1**), $\{(HMNA)_2 \cdot (H_2O)\}$ (**2**), and $(PMT)_2$ (**3**), respectively, when dichloromethane/acetonitrile/methanol (**1**) or dichloromethane (**2,3**) were used as solvents.

Correspondence to: S. K. Hadjikakou; e-mail: shadjika@uoi.gr/
N. Hadjiliadis; e-mail: nhadjis@uoi.gr

Present address of G. J. Corban: Inorganic Chemistry Laboratory, Department of Chemistry, College of Science, UAE University, 17551, Al Ain, United Arab Emirates.

© 2012 Wiley Periodicals, Inc.

The reaction of di-iodine with the thiol PMTH and 2-mercapto-benzothiazole (MBZTH) yields the disulfide $(PMT)_2$ (**3**), and the di-iodine adduct of formula $\{[MBZTH-I_2] \cdot [MBZTH]_2\}$ (**4**), respectively. The reaction of di-iodine with 5-nitro-2-mercapto-benzimidazole (O_2N -MBZIMH) (**5**) in the presence of ferric trichloride hydrate ($FeCl_3 \cdot 6H_2O$), in a 6:3:1 (I_2 :thiol: $FeCl_3 \cdot 6H_2O$) molar ratio, results in cocrystal (**6**), which contain the desulfurated hydroxyl derivative O_2N -BZIMOH (**6a**) and unreacted O_2N -MBZIMH (**6b**) in a 3:1 molar ratio. The compounds were characterized by elemental analysis, FT-IR, and 1H NMR spectroscopy. The crystal structures of compounds **1–6** were also determined by X-ray crystallography. Cyclic voltammetry measurements showed that thiols with low oxidation potentials (<1.0 V) mainly form

disulfides upon a reaction with di-iodine, whereas those with higher oxidation potential form charge transfer (CT), resulting in desulfurated products, MBZIMH. However, in the case of O₂N-MBZIMH a desulfurated species was isolated. The formation of the final product also requires the presence of FeCl₃. © 2012 Wiley Periodicals, Inc. Heteroatom Chem 23:498–511, 2012; View this article online at wileyonlinelibrary.com. DOI 10.1002/hc.21042

INTRODUCTION

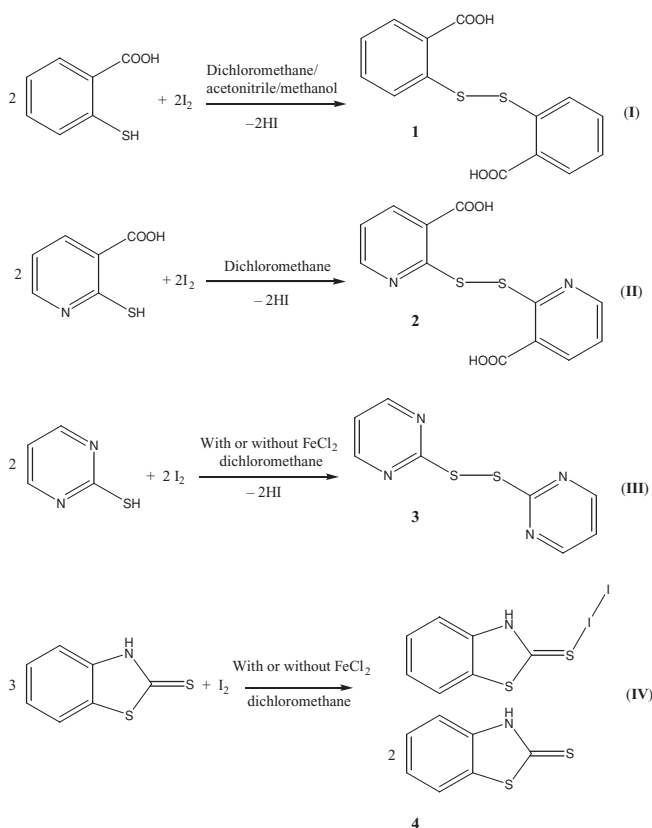
The study of a structure–activity relationship of thiols against di-iodine is stimulated, among other considerations, by the interest in the molecular compounds formed between antithyroid drugs and di-iodine [1–13], because thiols are known to exhibit antithyroid activity [13]. A variety of products, including charge transfer (CT) complexes, with “spoke structures” (D-I₂), “extended spoke structures” (D-I₂-I₂), iodonium salts [(L₂I)⁺(I_n)⁻], mono- and dicationic, and neutral disulfides [1–9,14–28] have been isolated from the reactions of di-iodine with thiols. The most commonly employed antithyroid drugs in use are 6-*n*-propyl-thiouracil (PTU), *N*-methylimidazole-2-thione (methimazole), and 3-methyl-2-thioxo-4-imidazole-1-carboxylate (carbimazole) [13]. Thyroid-peroxidase, a heme enzyme [29,30], which contains Fe(III) ions, is responsible for the oxidation of iodide anions to activate di-iodine [31–33]. Consequently, the study of the reaction of di-iodine with thiols in the presence of ferric or ferrous cations is of special interest.

Herein, we report the results of an investigation of the reaction of di-iodine with 2-mercapto-benzoic acid (H₂MBA), 2-mercapto-nicotinic acid (H₂MNA), and 2-mercapto-pyrimidine (PMTH), which resulted in the formation of the neutral di-sulfides of formulae {(HMBA)₂·(CH₃CN)} (1), {(HMNA)₂·(H₂O)} (2), and (PMT)₂ (3), respectively. Also described is the reaction of di-iodine with the thiols PMTH and 2-mercapto-benzothiazole (MBZTH) in the presence or absence of FeCl₂ in a 1:2:2 (I₂:thiol:FeCl₂) molar ratio, which results in 3, i.e., free of iodine, and the di-iodine adduct of formula {[MBZTH-I₂]₂·[MBZTH]₂} (4). The reaction of di-iodine with 5-nitro-2-mercapto-benzimidazole (O₂N-MBZIMH) (5) in the presence of ferric trichloride hydrate (FeCl₃·6H₂O) in a 6:3:1 (I₂:thiol:FeCl₃·6H₂O) molar ratio is described. This provided a structure (6) that suggests the presence of O₂N-MBZIMH, namely O₂N-BZIMOH (6a) and unreacted O₂N-MBZIMH (6b) in a 3:1 molar ratio.

RESULTS AND DISCUSSION

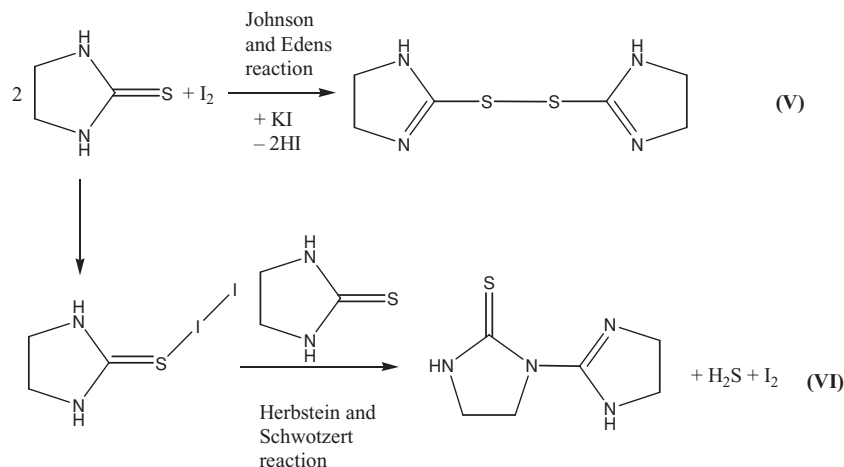
Reactions

We have previously shown that the reaction of di-iodine with 2-mercapto-pyridine (PYTH) led to the formation of a salt, which contained a monocationic disulfide and the I₃⁻ counteranion [1c]. Here, we extended our studies to the reactions of H₂MBA, H₂MNA, and PMTH with di-iodine in 1:2 (thiol:I₂) molar ratios. The neutral di-sulfides of formulae {(HMBA)₂·(CH₃CN)} (1), {(HMNA)₂·(H₂O)} (2), and (PMT)₂ (3) were thus formed, respectively (reactions I)–(III)). The same products were also obtained in the presence of FeCl₂ in a molar ratio 2:1:2 (thiol:I₂:FeCl₂).



When MBZTH was used for the reaction with di-iodines, the di-iodine adduct of formula {[MBZTH-I₂]₂·[MBZTH]₂} (4) (reaction (IV)) was formed.

Johnson and Edens [34] reacted ethylenethiourea with di-iodine in water, and they formulated the (red crystalline) product as the di-sulfide (Scheme 1 (V)). The repetition of this reaction by Herbstein and Schwotzer [35] showed that a condensation product was unexpectedly formed, by the N-substitution of ethylenethiourea,

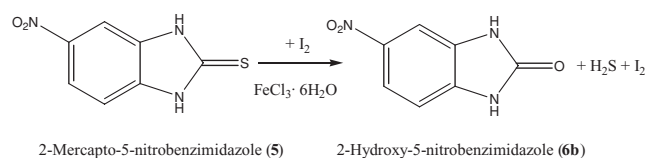


SCHEME 1

from its desulfurated species, indicating that a desulfuration of the thiol had taken place (Scheme 1 (VI)).

We have also recently shown that selenium analogues of the antithyroid drug PTU, of formulae RSeU [R = methyl- (Me-), ethyl- (Et-), *n*-propyl- (*n*-Pr-), and *i*-propyl- (*i*-Pr-)], reacted with diiodine in a 1:1 molar ratio in dichloromethane solutions and resulted in the formation of [(RSeU)₂I₂] [6]. Crystallization in chloroform led to the formation of the CT complex [(*n*-PrSeU)₂I₂]. Recrystallization of the [(RSeU)₂I₂] compounds in acetone afforded the diselenides of formulae [*N*-(6-Et-4-pyrimidone)(6-Et-SeU)₂] and [*N*-(6-*n*-Pr-4-pyrimidone)(6-*n*-Pr-SeU)₂]. Recrystallization in methanol/acetonitrile solutions, on the other hand, led to the deselenation with the formation of 6-*n*-propyl-2-uracil (*n*-Pr-U) [6]. The formation of these products indicated that deselenation occurred upon a reaction of selenoamides with di-iodine [6].

In this present work, similar to deselenation [6], the desulfuration of 2-mercapto-5-nitrobenzimidazole (**5**) upon a reaction with di-iodine was observed, producing 2-hydroxy-5-nitrobenzimidazole (**6a**) in the structure of cocrystal (**6**) (Scheme 2). This is the first reported example of such a reaction of a thiol in the presence of I₂.



SCHEME 2

Crystal and Molecular Structures of {(*HMBA*)₂·(*CH*₃*CN*)} (**1**), {(*HMNA*)₂·(*H*₂*O*)} (**2**), {(*PMT*)₂} (**3**), {[*MBZTH-I*₂]·[*MBZTH*]₂} (**4**), *O*₂*N-MBZIMH* (**5**), {*O*₂*N-BZIMOH*·*O*₂*N-MBZIMH*} (**6**)

Crystals of compounds **1–3**, suitable for a single crystal X-ray analysis, were grown by slow evaporation of the mother liquor remaining after filtration of the initial crops of solid material from the reactions of di-iodine with H₂MBA, H₂MNA, and PMTH in a molar ratio of 2:1, respectively, in dichloromethane/acetonitrile/methanol (**1**) or dichloromethane (**2,3**). Although the crystal and molecular structures of compounds **1–3** were reported previously [36–42], we have completed their structure determination here, to verify the formation of the disulfides from the reaction of thiols with di-iodine. Moreover, we were able to locate the disordered solvent–acetonitrile–molecule in the structure of **1**, while authors of the previous determination used the SQUEEZE procedure to help with the solvent-accessible space in the structure. The structure **2** is of superior quality (R = 0.0369) as compared to the previously reported one, which had a R factor of 7.28%. Table 1 summarizes the unit cell parameters and significant bond distances of the structures of the disulfides of **1–3** and their preparation conditions. The S–S bond distances in neutral disulfides **1–3** lie in the range of 2.043–2.045 Å in **1**, 2.0336–2.038 Å in **2**, and 2.013–2.020 Å in **3**.

Crystals of the {[*MBZTH-I*₂]·[*MBZTH*]₂} (**4**) were prepared according to reaction (IV). The atom-labeling scheme and selected geometric parameters for **4** are shown in Fig. 1 and Table 2, respectively.

TABLE 1 Unit Cell Parameters and Significant Bond Distances and Angles of the Reported Structures for the Disulfides 1–3

Complex	Unit Cell		Space Group	$d(S \cdots S)$ (Å)	$d(C \cdots S)$ (Å)	Preparation Method	References
	a, b, c (Å)	α, β, γ (°)					
1	16.733(5), 12.781(4), 21.091(6)	90, 107.52(3), 90, 1.784(3)	$C2/c$	2.0428(18), 2.0449(14)	1.784(3), 1.784(4),	H ₂ mba + 2I ₂ CH ₂ Cl ₂ / MeOH/MeCN	This work
IKIJER	16.446(0), 12.809(0), 20.954(0)	90, 104.56(0), 90	$C2/c$	2.043, 2.045	1.780, 1.779, 1.785	H ₂ mba + CH ₃ COOAg hydrothermal	[8a]
MUFNIK	9.208(0), 13.255(0), 17.893(0)	90, 93.39(0), 90	$P2_1/c$	2.057	1.795, 1.794	(Hmba)+ bipyridine MeOH	[8b]
WIKNOT	17.223(6), 12.904(6), 21.073(4)	90, 107.44(2), 90	$C2/c$	2.053, 2.045	1.800, 1.803, 1.790	Commercially purchased	[8c]
2	5.5950(10), 30.480(6), 8.084(2)	90, 102.08(3), 90	$P2_1/c$	2.0336(7)	1.7831(19), 1.7937(19)	H ₂ mna + 2I ₂ dichloromethane	This work
WUBZUO	5.5590(16), 30.227(14), 8.0589(6)	90, 101.874(2), 90	$P2_1/c$	2.038	1.791, 1.786	Not available	[9]
3	7.0280(10), 9.6690(10), 15.000(2)	86.46, 81.150(10), 79.990(10)	$P\bar{1}$	2.016, 2.020	1.776, 1.772, 1.768, 1.782	pmtH+ 2I ₂ dichloromethane	This work
3'	7.0397(7), 9.6707(9), 15.0053(16)	86.432(8), 81.153(8), 79.992(8)	$P\bar{1}$	2.0141(10), 2.0120(12)	1.770(3), 1.777(3), 1.781(3), 1.779(3)	2pmtH+ I ₂ + 2 FeCl ₂ dichloromethane	This work
PYMDSO	11.835(4), 6.994(1), 18.655(3)	90, 128.94(1), 90	$P2_1/c$	2.017	1.789, 1.781	pmtH water/NH ₃	[10a]
PYMDSO1	11.824(1), 6.9357(6), 14.4896(12)	90, 90.423(2), 90	$P2_1/n$	2.015	1.778, 1.781	pmtH + Bi(OH) ₃ water/NH ₃	[10b]
PYMSUL10	9.673(5), 15.033(6), 7.045(3)	98.73(3), 100.02(4), 86.45(4)	$P\bar{1}$	2.018, 2.020	1.1786, 1.782, 1.182, 1.777	pmtH + Cu ²⁺ water/NH ₃	[10c]

Cocrystal **4** comprises three components; one CT di-iodine-thiols residue and two neutral thiol ligands (molecules, i.e., *a*, *b*, and *c*; see Fig. 1). The closest S1⋯S1 distance between the neutral thiol ligands is 3.921(3) Å slightly shorter than the double the van der Waals radius of S atom (1.8–2.06 Å) [43], indicating a very weak S⋯S interaction. This is further supported by the lengthening of C–S bond distances of this constituents (molecule *b*: 1.671(8) Å and molecule *c*: 1.681(7) Å) in contrast to the free ligand (1.657 Å [44], 1.660 Å [45]). The three components of **4**, *a*, *b* and *c*, are each planar with mean deviations from their least-square planes being 0.021(7), 0.016(8), and 0.022(7) Å, respectively. In the CT complex, this planarity extends to include the I₂ residue as seen in the I1/S1/C1/S2 and I1/S1/C1/N1 torsion angles of 7.9(5) and –175.8(5)°, respectively. An almost linear geometry is found in

I2-I1-S1, with the angle at I1 of 176.95(4)°. Owing to the kink in the molecule due to the I1-S1-C1 link [104.2(2)°], an intramolecular I1⋯S2 separation of 3.588(2) Å is noted. A comparison of the bond distances defining the three MBZTH molecules shows that the values for those associated with the coordinated MBZTH molecule lie in the range found for the noncoordinated molecules. In the same way, the angles are equal within experimental error with the notable exception of the S1–C1–S2 and S1–C1–N1 angles that appear to increase and decrease, respectively, by a few degrees upon coordination of LH to I₂ (Table 2). As may also be seen from Fig. 1, the three molecules are effectively coplanar in the crystal structure. Thus, the sequence of dihedral angles between molecules *a*, *b*, and *c* is *a/b* 6.9(2), *a/c* 5.5(2), and *b/c* 2.2(2)°, respectively. This arrangement allows for the formation of N–H⋯S

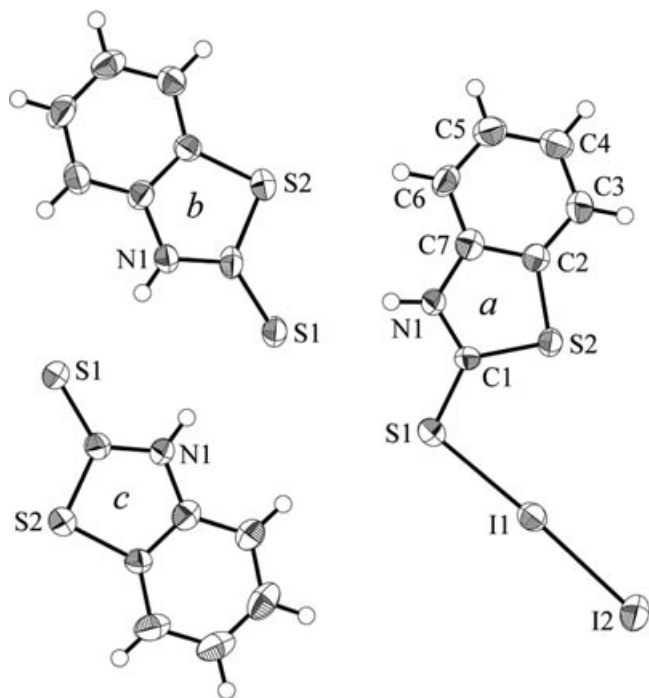


FIGURE 1 Molecular structure of the CT complex **4** showing the crystallographic numbering scheme employed.

hydrogen-bonding interactions between these molecules. Data for the most significant hydrogen-bonding interactions are summarized in Table 3. The three-molecule aggregates are sustained by N–H···S interactions, shown as a, b and c in Fig. 2, associate via a number of C–H···S and C–H···I interactions with adjacent three-molecule aggregates to form a layer structure with the closest of these highlighted in the Fig. 3 as d and e, respectively. The layers thus formed stack parallel to (110) via π ··· π interactions with the closest such interaction of 3.445(4) Å, occurring between the ring centroids of the S2a–C2a and C2c–C7c rings.

The I1–I2 bond is 2.8719(9) Å is longer than I–I bond distance of free di-iodine (2.717 Å) [46] as a result of the intramolecular S···I interaction. We have previously reported the structure of the CT complexes of formulae [MBZTH–I₂][·] and [MBZTH–I₂·I₂] with the so called “spoke” and “extended spoke” arrangements [1]. The corresponding I–I bond distances were 2.969(2) Å in [MBZTH–I₂][·] and 3.077(2) Å in [MBZTH–I₂·I₂] with the latter being among the longest such bond distance ever measured in this class of compound [1]. The I1–S1 bond was 2.684(2) Å, whereas the corresponding bond distance in complexes [MBZTH–I₂][·] and [MBZTH–I₂·I₂] was 2.587(5) and 2.728(6) Å, respectively.

The I–I bond order (*n*) calculated by Pauling’s equation [1,47] is 0.579, classifying this adduct as

TABLE 2 Selected Geometric Parameters^o for **4**^a

Bond	Molecule a	Molecule b	Molecule c
Bond distance (Å)			
S1–C1	1.679(6)	1.671(8)	1.681(7)
S2–C1	1.728(7)	1.736(8)	1.718(7)
S2–C2	1.750(7)	1.740(7)	1.760(7)
N1–C1	1.346(8)	1.356(9)	1.340(9)
N1–C7	1.395(9)	1.397(9)	1.391(9)
Bond angles (°)			
S1–C1–S2	126.6(4)	124.7(4)	122.8(5)
S1–C1–N1	122.8(5)	125.4(6)	125.2(5)
S2–C1–N1	110.5(5)	110.0(5)	111.0(5)
C1–S2–C2	91.4(3)	92.2(3)	91.7(3)
C1–N1–C7	116.1(6)	115.3(6)	115.5(6)
I1–I2	2.8719(9)		
I1–S1	2.684(2)		
I2–I1–S1	176.95(4)		
I1–S1–C1	104.2(2)		

^aI1–I2 = 2.8719(9), I1–S1 = 2.684(2) Å, I2–I1–S1 = 176.95(4), I1–S1–C1 = 104.2(2)°.

an intermediate **B**-type adduct complex (D–I–I); **A**-type complexes correspond to D···I–I with an I–I bond order ≥ 0.6 and $d(\text{I–I}) < 2.85$ Å, whereas **C**-type compounds are best described as D–I···I with $n \leq 0.4$, ($d(\text{I–I}) > 3.01$ Å) [48,49].

The variations in the I–I and S–I bond distances between the thiol–I₂ adduct in **4** and those reported previously in complexes [MBZTH–I₂][·] and [MBZTH–I₂·I₂] result from intermolecular interactions between the coordinated and uncoordinated MBZTH molecules described above.

Slow evaporation of the filtrate of the reaction mixture of di-iodine with O₂N–MBZIMH (**5**) in the presence of FeCl₃·6H₂O in a 6:3:1 (I₂:thiol:FeCl₃·6H₂O) molar ratio in dichloromethane gave crystals suitable for X-ray work. Figure 3A shows its crystal and molecular structure. Desulfuration of 2-mercapto-5-nitrobenzimidazole (**5**) upon a reaction with di-iodine resulted in a cocrystal (**6**), which contains a mixture of desulfurated O₂N–BZIMOH (**6a**) and O₂N–MBZIMH (**6b**) in a 3:1 ratio. The structures of **5** and **6** were determined at low levels of precision owing to the poor quality of the crystals obtained. Accordingly, discussion is restricted to the nature of their chemical composition, which has been independently verified by spectroscopy. Molecular diagrams of **5** and **6a** (i.e., in the structure of (**6**)) are given in Figs. 3A and 3B). Attempts to isolate the desulfurated **6a** product from the reaction in the absence of FeCl₃ were unsuccessful, and this emphasizes the role of the iron salt in the reaction, possibly acting as a catalyst.

TABLE 3 Hydrogen-Bonding Parameters Operating in the Structure of 4

$A-H \cdots B$	$A-H$ (Å)	$H \cdots B$ (Å)	$A \cdots B$ (Å)	$\angle A-H \cdots B$ (°)	Symmetry Operation
$N1a-H1a \cdots S1b$	0.87	2.61	3.388(6)	150	x, y, z
$N1b-H1b \cdots S1c$	0.87	2.44	3.296(6)	166	x, y, z
$N1c-H1c \cdots S1b$	0.87	2.51	3.373(6)	169	x, y, z
$C3a-H3a \cdots S1c$	0.94	2.80	3.567(8)	140	$-1 + x, y, 1 + z$
$C3b-H3b \cdots I_2$	0.94	3.05	3.927(7)	157	$1 + x, -1 + y, z$

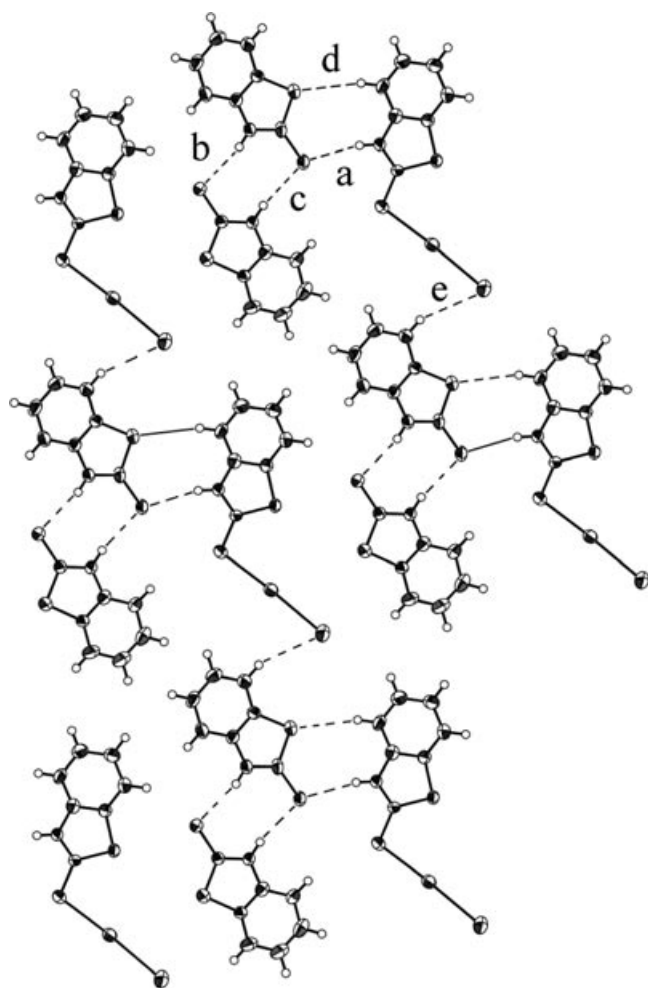


FIGURE 2 A view of the supramolecular aggregation operating in the crystal structure of 4.

The C–O bond length in **6a** is 1.255(15) Å, whereas the S–C bond distance of **6b** is 1.777(16) Å. The corresponding C–S bond distance in free O₂N-MBZIM (**5**) is 1.673(7) Å. The lengthening of the C–S bond in the case of **5b** as compared with that of the starting free ligand **5** may indicate the involvement of a disulfide species in the desulfuration process. The C(7A)–N(1)–C(2)–O(2) and C(3A)–N(3)–C(2)–

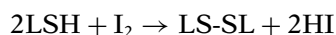
O(2) torsion angles for complex **6a** are 179.1(6)° and –179.7(5)°, respectively, which substantiates the planar arrangement with corresponding angles of 122.2(10)° and O(2)–C(2)–N(3) = 131.3(10)°.

The constituent atoms of **5a** associate via N–H···O interactions with the closest ones being 1.94 Å between O(1W) and H(3) and 2.00 Å between O(2) and H(1) (–1 –x, 2 –y, 1 –z), and a weaker interaction corresponding to C(4)–H(4)···O(52) with H(4)···O(52) (1 –x, –1/2 + y, 3/2 –z) = 2.37 Å

Computational Studies

To investigate the possible reaction paths for the oxidation reaction of the various ligands reacting with di-iodine, computational studies were carried out. The disulfides of H₂MBA, H₂MNA, and PMTH were formed together with the spoke CT complex in the case of MBZTH, and the formation of the hydroxyl derivative from O₂N-MBZIM was analyzed in these computations.

The oxidation potentials of the thiol H₂MBA, H₂MNA, PMTH, MBZTH, and O₂N-MBZIMH were calculated from the free energy (ΔG) of the oxidation reaction (reaction (V)).



where LSH = H₂MBA, H₂MNA, PMTH, MBZTH, and O₂N-MBZIMH (V)

The calculated values for the free energy (ΔG) are 8.54 kcal/mol for H₂MBA, 11.74 kcal/mol for H₂MNA, 12.81 kcal/mol for PMTH, 15.77 kcal/mol for MBZTH, and 20.82 kcal/mol for O₂N-MBZIMH, whereas the average S–S lengths of the corresponding disulfides increase in the order 2.047, 2.035, 2.016, and 3.921 Å, respectively, for H₂MBA, H₂MNA, PMTH, and MBZTH. These outcomes indicate that the higher the free energy of the oxidation reaction the longer S–S bond distance is. This supports further our assumptions from the crystal structures. The free energy was also calculated for the ligand O₂N-MBZIMH, assuming the formation of a disulfide (ΔG = 20.82 kcal/mol. Intermediate free energy values of the ligands, as in the

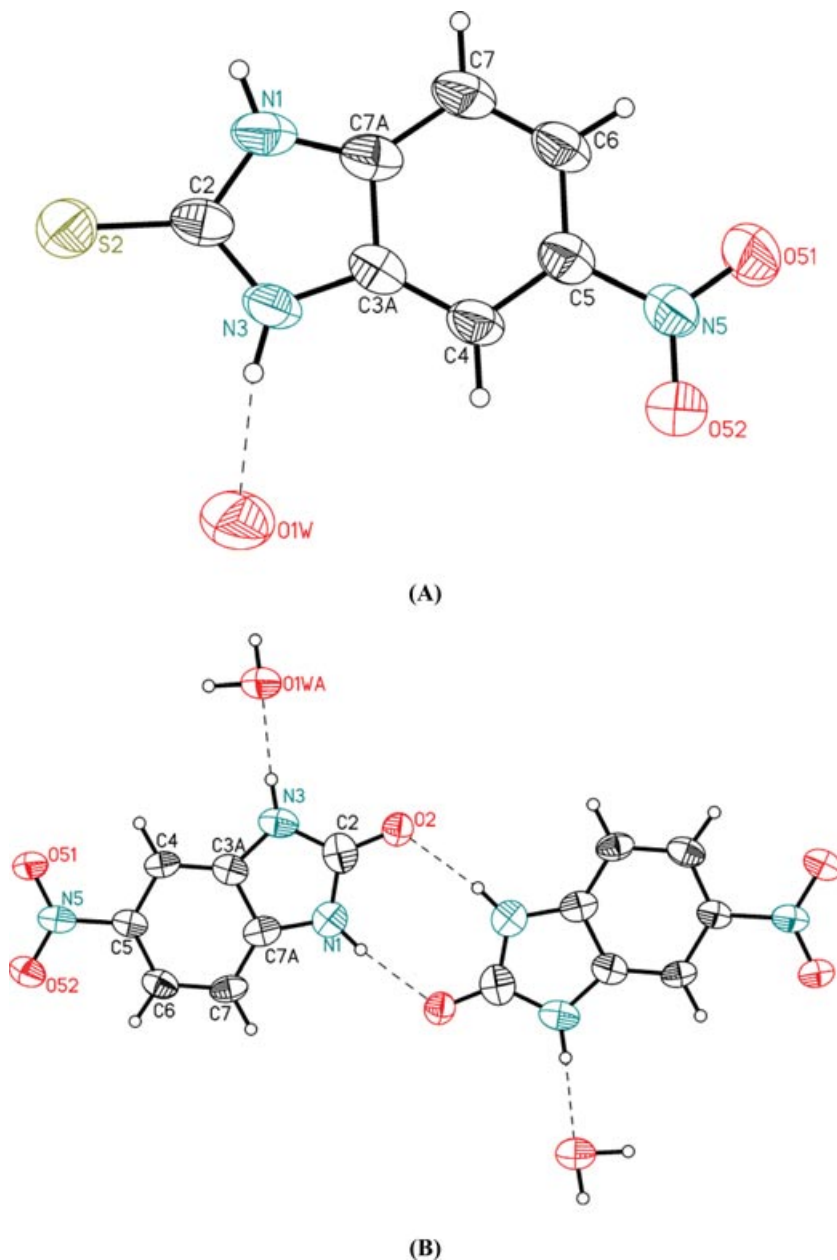
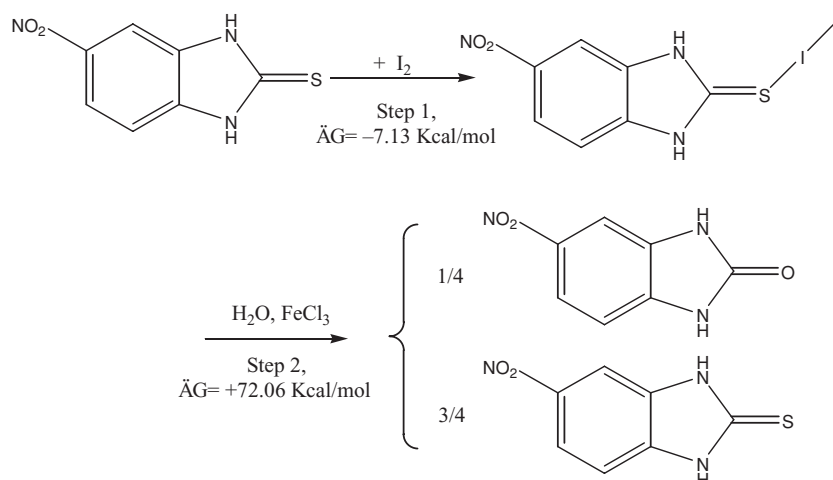


FIGURE 3 (A) Molecular structure of the **5-H₂O**. Selected bond lengths (Å) and angles (°): C2–S2 = 1.673(7), N1–C2 = 1.346(8), C2–N3 = 1.357(8), C5–N5 = 1.457(9), N5–O51 = 1.228(7), N5–O52 = 1.218(7), N3–C2–N1 = 105.5(6), N3–C2–S2 = 127.3(5), N1–C2–S2 = 127.2(5), O51–N5–O52 = 122.6(6), O52–N5–C5 = 118.6(6), O51–N5–C5 = 118.8(6). (B) The hydroxyl derivative O₂N-BZIMH (**6a**), which coexists with O₂N-MBZIMH (**6b**) in the crystal of **6a-6b**. The **6b** is not shown for clarity. C2–O2 = 1.255(15) (**6a**), C2–S2' = 1.777(16) (**6b**), N1–C2 = 1.370(12), C2–N3 = 1.380(11), C5–N5 = 1.492(10), N5–O51 = 1.215(8), N5–O52 = 1.240(7), O2–C2–N3 = 131.3(10) (**6a**), O2–C2–N1 = 122.2(11) (**6a**), N3–C2–S2' = 114.0(8) (**6b**), N1–C2–S2' = 139.3(8) (**6b**), N3–C2–N1 = 106.6(7), O51–N5–O52 = 123.9(7), O52–N5–C5 = 117.0(6), O51–N5–C5 = 119.0(6).

case of MBZTH, may lead to CT complexes. Finally, the highest energy values were calculated for O₂N-MBZIMH, which could explain its further oxidation and the formation of the hydroxyl derivatives (Scheme 3). Based on our results, the following re-

action pathway may be proposed for the reaction of O₂N-MBZIMH with I₂ and FeCl₃, leading to the desulfurated products (Path: first step $\Delta G = -7.13$ kcal/mol, second step $\Delta G = +72.06$ kcal/mol; total $\Delta G = +63.93$ kcal/mol). A consideration of other



SCHEME 3

possible mechanisms through the disulfide and the direct transformation of the CT complex to the desulfurated one were excluded owing to unrealistic ΔG values.

Electrochemical Studies

To further examine the influence of the redox potential on the structure of the thiol-di-iodine derivatives, the redox properties of compounds H₂MBA, PYTH, PMTH, 2-mercapto-benzimidazole (MBZIMH), O₂N-MBZIMH, MBZTH, and 2-mercaptothiazolidine (MTZDH) were investigated by means of cyclic voltammetry (CVA) and differential pulse voltammetry (DPV) [50]. The CV measurements were performed in a solution of *n*-Bu₄NBF₄ in anhydrous CH₂Cl₂ and DMF. The experimental electrochemical redox potential data for the ligands studied here are summarized in Table 4 and compared to the

calculated oxidation potentials from the free energy calculated for their oxidation reactions.

A representative cyclic voltammogram, of H₂MBA, in the anodic range in CH₂Cl₂ is presented in Fig. 4A. The one-electron irreversible peak controlled by diffusion (the dependence of *I* vs. *v*^{1/2} has a linear character) at *E*_p = 1.22 V obviously corresponds to the thiol group oxidation [51]. This process results in the formation of a radical cation. This is followed by the fast (on the voltammetric timescale) deprotonation and the formation of a radical (Scheme 4), which may be involved in further chemical transformations (dimerization, etc.) [52].

There are two reduction peaks observed for H₂MBA in CH₂Cl₂. It is well known that the potential of proton reduction in acidic groups strongly depends on the value of p*K*_a [53]. This value for the carboxyl moiety is lower than that for the SH group. Therefore, a CVA curve displays two waves of

TABLE 4 Electrochemical Properties of Ligands 1–7 in CH₂Cl₂ and DMF^a

Compound	Oxidation Potentials, V Experimental		Reduction Potentials, V Experimental		Oxidation potentials, V calculated
	CH ₂ Cl ₂	DMF	CH ₂ Cl ₂	DMF	
1 PYTH	0.37, 0.55	0.51, 0.64	-1.61	1.45	
2 H ₂ MBA	1.22	1.26	-0.75, -1.29	-0.75, -1.17	-0.37
3 H ₂ MNA		0.90 ^b		-1.20 ^b	-0.51
3 PMTH,	0.47, 0.84	0.68, 0.90/0.75	-1.43	-1.35	-0.56
4 MBZIMH	1.18	1.35	-1.10	-1.15	
5 O ₂ N-MBZIMH	1.24	1.26	-1.1, -1.51	-1.15, -1.4	-0.90
6 MBZTH	1.2	1.36	-1.37	-1.35	-0.68
7 MTZDH	1.23	1.26	-1.34	-1.15	

^aRedox potentials (V vs. Ag/AgCl/KCl) were determined from cyclic voltammetric scans. Experimental conditions: Pt electrode, *v* = 200 mV/s, 293 K, 50 mM *n*-Bu₄NBF₄, *E*_p denotes peak potential of a chemically irreversible step.

^bRedox potential (V vs. SCE) in DMSO [11b].

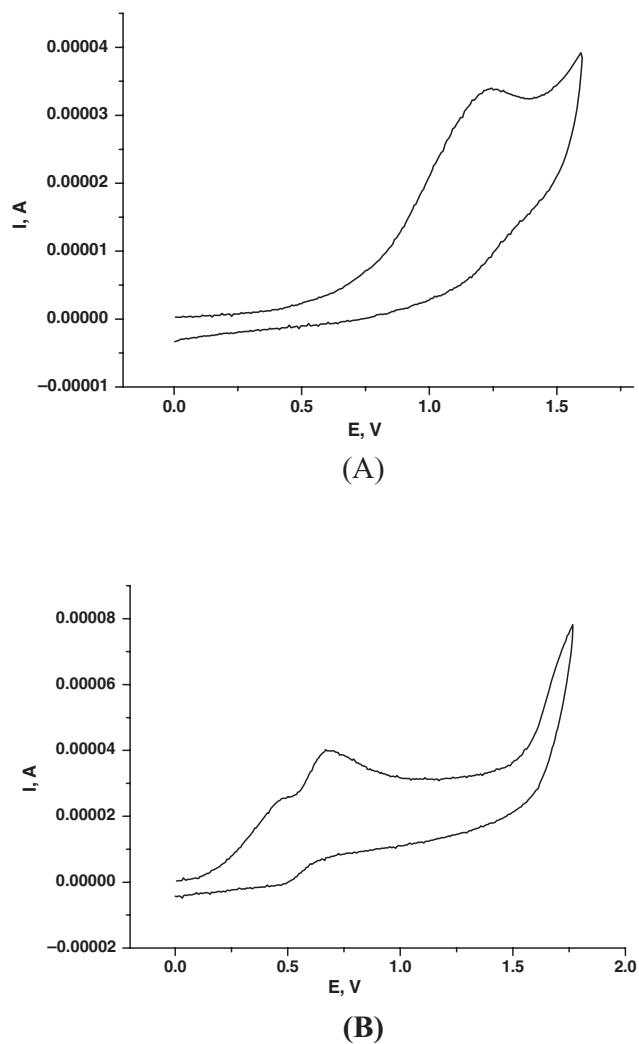
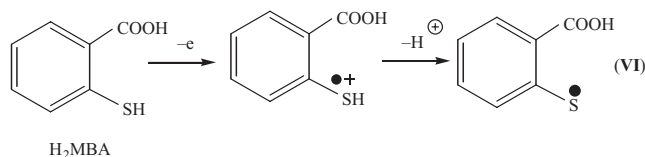


FIGURE 4 Cyclic voltammogram oxidation at 293 K (CH_2Cl_2 , scan rate 200 mV/s, Pt, 10^{-3} M, 50 mM *n*-Bu₄NBF₄, vs. Ag/AgCl/KCl) of H₂MBA (A) and PYTH (B).



SCHEME 4

reduction: first at $E_p = -0.75$ V, which is attributed to the reduction of the carboxyl group proton, the next step at $E_p = -1.29$ V, which may be assigned to the reduction of the SH group.

There are several redox-active sites in compounds PYTH, PMTH, MBZIMH, O₂N-MBZIMH, MBZTH, and MTZDH. They all exist in thiol (**a**) and thione (**b**) tautomeric forms. The oxidation or reduc-

tion can proceed with the participation of N, NH, and SH groups, depending on the nature of these tautomeric forms.

Using the CVA method, we can make some assumptions concerning the redox-active forms of these compounds. For example, the cyclic voltammogram of PYTH in CH_2Cl_2 shows two one-electron irreversible peaks of oxidation (Fig. 4B). The second peak is lower than the first one, and the ratio I_{p1}/I_{p2} depends on the scan rate. This observation indicates that the second oxidation process is connected with the first. We can attribute the second wave to oxidation of a product, which is formed in the first oxidation process.

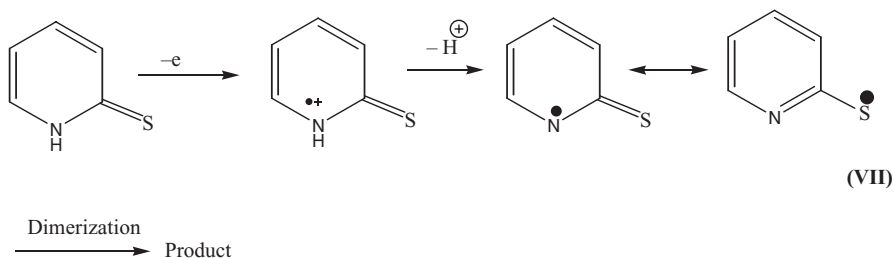
Thus, in this case the electrochemical mechanism takes place. We assume that compound PYTH exists in the tautomeric form **b** (thione), which is oxidized at $E_p = 0.37$ V (Scheme 5).

This wave may be associated with the NH fragment oxidation, which results in the formation of the corresponding N-centered radical cation, followed by a rapid (in CVA timescale) deprotonation. The radical formed in this process is involved in chemical reactions (for instance, dimerization) and the second oxidation peak at $E = 0.49$ V corresponds to their product oxidation. The small difference in the oxidation potential suggests that the electroactive centers have similar characteristics (obviously, the NH-oxidation in tautomer **b** dimer) [54]. If the assumption that PYTH in CH_2Cl_2 exists in the form of tautomer **b** is correct, then the peak in the reduction side must be shifted to the cathodic range (because of the weaker acidic properties of tautomer **b** (thione) than of H₂MBA). Experimental data support this assumption: The reduction of PYTH proceeds at more negative potential than in the case of H₂MBA.

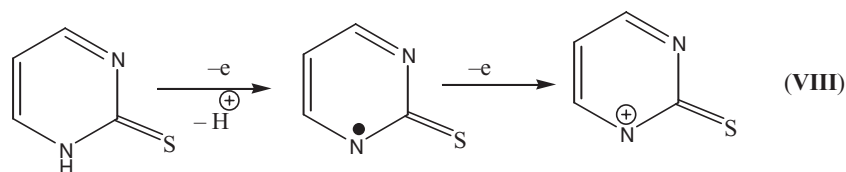
The structure of PMTH is similar to PYTH, and their electrochemical behavior is analogous. On CVA, two one-electron waves at $E_p = 0.47$ V, $E_{p2} = 0.84$ V, respectively, appear in the anodic range. The oxidation potentials of PMTH are shifted toward more positive side according to the literature data [55].

In this case, the difference between the first and the second oxidation peaks is more significant than in the case of PYTH. This indicates that the nature of the first wave is the same (N-centered oxidation followed by the fast deprotonation with the formation of a radical); the second step is different (Scheme 6). Probably, in this case the radical is stabilized due to delocalization and the oxidation proceeds at more positive potentials.

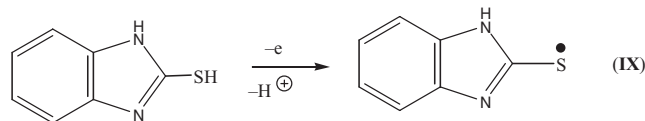
The irreversible wave is observed in the cathodic range. The potentials of PYTH and PMTH reductions



SCHEME 5



SCHEME 6



SCHEME 7

are comparable. Therefore, it is concluded that the mechanism of reduction is also similar.

The electrochemical behavior of MBZIM is different. This compound shows a one-electron irreversible wave that can be attributed to SH oxidation (Scheme 7).

It is probable in this case that the conjugation with the benzene ring leads to the stabilization of the tautomeric form **a**. In the cathodic range, this compound displays an irreversible wave at $E_p = -1.10$ V that corresponds to the reduction of the SH group as was shown previously [56]. The redox behavior of the compounds MBZIMH, O₂N-MBZIMH, and MBZTH is analogous (Table 4).

The cyclic voltammogram of MTZDH shows one-electron redox process at $E_p = 1.23$ V assigned to the SH group oxidation. In the cathodic range, one irreversible wave of SH reduction is observed. Thus, it can be proposed that this compound also exists in the tautomeric form **a**.

The electrochemical behavior of the studied compounds in DMF is analogous: Compounds PYTH and PMTH exist in the tautomeric form **b**, and their oxidation proceeds in two steps (Fig. 5A). In this case, the second peak of PYTH oxidation is even slightly pronounced than in the case of

CH₂Cl₂. Its existence is proven by means of DPV (Fig. 5B). It can be seen that two peaks of PYTH oxidation are observed. Compounds MBZIMH, O₂N-MBZIMH, MBZTH, and MTZDH in DMF exist in the tautomeric form **a**. Voltammograms of these compounds show an one-electron wave in the anodic range corresponding to the SH-group oxidation (Fig. 6, Table 4).

CONCLUSIONS

The chemical reactivity of di-iodine toward the thiols H₂MBA, H₂MNA, PMTH, MBZTH, and O₂N-MBZIMH in the presence and absence of Fe(II)/Fe(III) ions was investigated. The crystal structures of the reaction products reveal that the reaction of di-iodine with the thiols H₂MBA, H₂MNA, and PMTH produces disulfides with S–S bond distances dependent on the oxidation ability of the ligand. In the case of MBZTH, the compound {[MBZTH-I₂]:[MBZTH]₂} (**4**) is isolated in which the S–S distance is 3.921(3) Å, which might indicate a weak S··S interaction. In the case of O₂N-MBZIMH (**5**), the desulfurated product O₂N-BZIMOH (**6a**), isolated in its 3:1 cocrystal with O₂N-MBZIMH (**5**), is the final product obtained upon its reaction with di-iodine. The desulfuration mechanism involved the formation of a CT spoke complex, which is consequently hydrolyzed into the corresponding hydroxyl derivative.

CVA measurements (Table 4) showed that thiols with low oxidation potential (<1.0 V) mainly form disulfides upon oxidation with di-iodine as an oxidizing agent, whereas those with higher oxidation

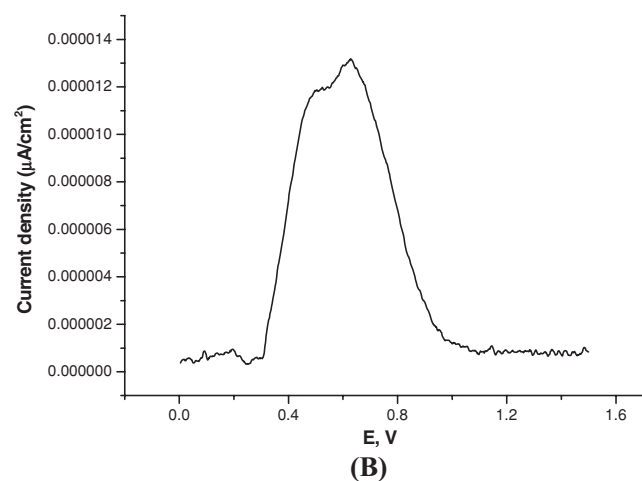
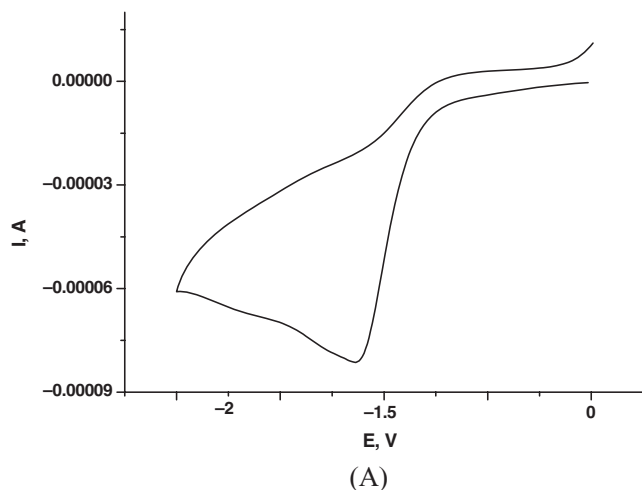


FIGURE 5 (A) Cyclic voltammogram reduction of PYTH at 293 K (CH_2Cl_2 , scan rate 200 mV/s, Pt, 10^{-3} M, 50 mM $n\text{-Bu}_4\text{NBF}_4$, vs. Ag/AgCl/KCl). (B) Differential-pulse voltammogram of PYTH (DMF, Pt, 10^{-3} M, 50 mM $n\text{-Bu}_4\text{NBF}_4$, vs. Ag/AgCl/KCl).

potential form CT complexes with “spoke” or “extended spoke” structures when they react with diiodine. The only exception is $\text{O}_2\text{N-MBZIMH}$, where a desulfurated species was isolated. The computational study on the H_2MBA , H_2MNA , and PMTH molecules, with oxidation potentials -0.37 to -0.56 V, shows they form the disulfides, whereas the MBZTH (-0.68 V) forms the CT spoke structure, and the one species with the lower oxidation potential (-0.90 V) forms the desulfurated product.

EXPERIMENTAL

Materials and Instruments

All solvents used were of reagent grade. Di-iodine (Aldrich), H_2MBA , H_2MNA , PMTH, MBZTH, and

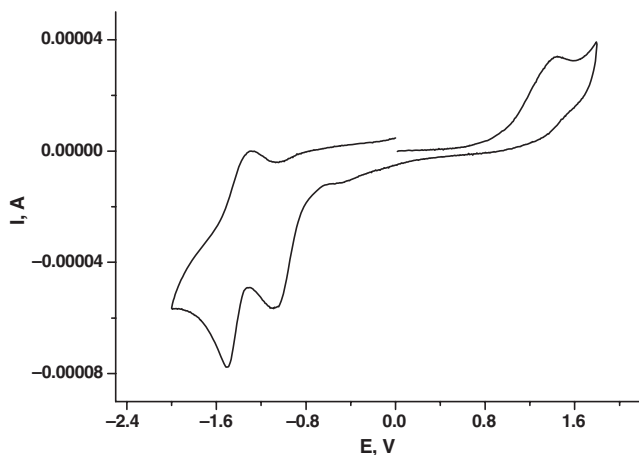


FIGURE 6 Cyclic voltammogram of MBZIMH (DMF, scan rate 200 mV/s, Pt, 10^{-3} M, 50 mM $n\text{-Bu}_4\text{NBF}_4$, vs. Ag/AgCl/KCl).

$\text{O}_2\text{N-MBZIMH}$ (Aldrich, Merck) were used with no further purification. Elemental analyses for C, H, N, and S were carried out with a Carlo Erba EA model 1108 elemental analyzer. Melting points were measured in open tubes with a Stuart scientific apparatus and are uncorrected. Infrared spectra in the region of $4000\text{--}370\text{ cm}^{-1}$ were obtained in KBr disks, whereas far infrared spectra in the region of $400\text{--}50\text{ cm}^{-1}$ were obtained in polyethylene disks, with a Perkin-Elmer spectrum GX FT-IR spectrophotometer. A Jasco UV/Vis/NIR V 570 series spectrophotometer was used to obtain the electronic absorption spectra. The ^1H NMR spectra were recorded on a Bruker AC250 MHFT NMR instrument in $\text{MeOH-}d_3$, CDCl_3 solutions. Chemical shifts δ are given in ppm with internal ^1H TMS.

Synthesis and Crystallization of $\{(\text{HMBA})_2 \cdot (\text{CH}_3\text{CN})\}$ (1), $\{(\text{HMNA})_2 \cdot (\text{H}_2\text{O})\}$ (2), $\{(\text{PMT})_2\}$ (3), $\{[\text{MBZTH-I}_2] \cdot [\text{MBZTH}]_2\}$ (4), $(\text{O}_2\text{N-MBZIMH} \cdot \text{H}_2\text{O})$ (5), and $(\text{O}_2\text{N-BZIMOH} \cdot \text{O}_2\text{N-MBZIMH} (3/1))$ (6)

Compounds **1–3** were synthesized from the reaction of 0.5 mmol of the ligands (0.077 g H_2MBA , 0.077 g H_2MNA , and 0.055 g PMTH) with 1 mmol I_2 (0.254 g) in dichloromethane/acetonitrile/methanol (**1**) or dichloromethane (**2,3**) at 0°C . The reaction of di-iodine with the thiols PMTH and MBZTH in the presence of FeCl_2 in a 1:2:2 (I_2 :thiol: FeCl_2) molar ratio produced the compound **3** and **4**. Crystals of **5** were grown from its dichloromethane solution. Slow evaporation of the filtrate derived from the reaction of di-iodine with $\text{O}_2\text{N-MBZIMH}$ (**5**) in the presence

of $\text{FeCl}_3 \cdot 6\text{H}_2\text{O}$ in a 6:3:1 (I₂:thiol: $\text{FeCl}_3 \cdot 6\text{H}_2\text{O}$) molar ratio in dichloromethane produced **6**.

- 1**: yield 8.5% corresponding to 0.022 g of product; mp 165–168°C. Elemental analysis, found: C 55.43, H 3.35, N 0.80, S 20.15; calcd: C 55.63, H 3.18, N 0.74, S 20.25. MID-IR (KBr) (cm^{-1}): 3059w, 2656m, 1680vs, 1586m, 1560s, 1461s, 1415vs, 1261vs, 1150m, 1036m, 897m, 807m, 739vs, 693m, 649m, 551m. ¹H NMR (CDCl_3) (δ ppm): 8.36s, 8.08–8.04d, 7.67–7.64d, 7.62–7.58d, 7.41–7.35t.
- 2**: yield 20% corresponding to 0.061 g of product; mp 225–228°C. Elemental analysis, found: C 46.35; H 2.52; N 9.17; S 20.43; calcd: C 46.75; H 2.61; N 9.09; S 20.80. MID-IR (KBr) (cm^{-1}): 3076w, 1558vs, 1252m, 1136m, 701s
- 3**: yield 20% corresponding to 0.044 g of product; mp 93–97°C. Elemental analysis, found: C 34.75; H 2.19; N 20.04; S 21.65; calcd: C 34.89; H 2.23; N 20.53; S 21.34. MID-IR (KBr) (cm^{-1}): 3065w, 1556vs, 1376vs, 1166 vs, 743s ¹H NMR (DMSO) (δ ppm): 8.56–8.58d, 7.05–7.09t
- 4**: yield 37.43% corresponding to 0.108 g of product; mp 120–125°C. Elemental analysis, found: C 34.53, H 1.95, N 5.73, S 24.69; calcd: C 33.38, H 2, N 5.56, S 25.46. MID-IR (KBr) (cm^{-1}): 3453b, 3114w, 3066w, 2960w, 2892w, 2360w, 1599m, 1492s, 1457m, 1427vs, 1324vs, 1248m, 1128w, 1077s, 1036vs, 1012s, 923w, 841w, 742vs, 670s, 599s, 564m, 495w. ¹H NMR (DMSO) (δ ppm): 10.51s-br, 7.62–7.59d, 7.56–7.51t, 7.51–7.47t, and 7.43–7.40d

Crystal Data

Data for compounds studied were collected by employing the ω scan technique in the θ range 2.55–25.00° (**1**), 5.16–29.25° (**2**), 2.50–29.00° (**3**), 2.50–25.00° (**3'**), 1.71–24.98° (**4**), 2.20–25.00° (**5**), and 4.80–70.00° (**6**) on an Agilent Technologies Xcalibur four-circle diffractometer [57] with Sapphire CCD detector (**1**, **2**, **3'**, **5** and **6**), on a Bruker P4 diffractometer (**3**) and on an Enraf Nonius FR590 diffractometer (**4**), all using graphite-monochromated Mo K_α ($\lambda = 0.71073 \text{ \AA}$) radiation. Data for the crystals of **6** were collected at 130(1) K on an Agilent Technologies Supernova diffractometer with an Atlas CCD detector, using Cu K_α ($\lambda = 1.54178 \text{ \AA}$) radiation.

Cell parameters for **1**, **2**, **3**, **3'**, **5**, and **6** were determined by least-square fit. All data were corrected for Lorentz-polarization effects and absorption [58]. The structures were solved with direct methods with SHELXS97 [59] and refined by full-matrix least-

square procedures on F^2 with SHELXL97 [60]. All non-hydrogen atoms were refined anisotropically; hydrogen atoms in **1**, **4**, **5**, and **6b** were located at calculated positions and refined as a “riding model” with isotropic thermal parameters fixed at 1.2 times the Ueq’s of appropriate carrier atom. In **2** and **3'**, hydrogen atoms were found in the difference Fourier maps and freely refined with isotropic displacement parameters.

The large residual electron density in **1** was interpreted as a disordered solvent–acetonitrile molecule; weak constraints have been applied to the geometry and displacement parameters of this fragment. The crystals of **5** were of inferior quality, the data allowed for successful refinement of the structure, but the water molecule hydrogen atoms were not located. The crystals of **6a–6b** were refined as twins. The structure of **4** was solved by using heavy atom methods [59] and refined [60] on F^2 with non-hydrogen atoms modeled with anisotropic displacement parameters, with hydrogen atoms in the riding model approximation and using a weighting scheme of the form $w = 1/[\sigma^2(F_o^2) + (0.1172P)^2]$, where $P = (F_o^2 + 2F_c^2)/3$. Significant crystal data are given below.

The structure of **4** was solved by employing heavy-atom methods [60] and refined [61] on F^2 with non-hydrogen atoms modeled with anisotropic displacement parameters, with hydrogen atoms in the riding model approximation and using a weighting scheme of the form $w = 1/[\sigma^2(F_o^2) + (0.1172P)^2]$, where $P = (F_o^2 + 2F_c^2)/3$. Significant crystal data are given below.

- 1**: $3(\text{C}_{14}\text{H}_{10}\text{O}_4\text{S}_2) \cdot \text{CH}_3\text{CN}$, MW = 953.13, monoclinic, space group $C2/c$, $a = 16.733(5)$, $b = 12.781(4)$, $c = 21.091(6) \text{ \AA}$, $\beta = 107.52(3)^\circ$, $V = 4302(2) \text{ \AA}^3$, $Z = 4$, $T = 295(2)$, $\rho(\text{calcd}) = 1.47 \text{ g cm}^{-3}$, $\mu = 0.38 \text{ mm}^{-1}$, $F(000) = 1970$. The refinement converged to final R [for 2571 reflections with $I > 2\sigma(I)$] = 0.057, $wR = 0.204$ (all 3608 reflections).
- 2**: $\text{C}_{12}\text{H}_8\text{N}_2\text{O}_4\text{S}_2 \cdot \text{H}_2\text{O}$, MW = 362.34, monoclinic, space group $P 2_1/c$, $a = 5.5950(10)$, $b = 30.480(6)$, $c = 8.084(2) \text{ \AA}$, $\beta = 102.08(3)^\circ$, $V = 1348.1(5) \text{ \AA}^3$, $Z = 4$, $T = 293(2)$, $\rho(\text{calcd}) = 1.61 \text{ g cm}^{-3}$, $\mu = 0.42 \text{ mm}^{-1}$, $F(000) = 672$. The refinement converged to final R [for 2671 reflections with $I > 2\sigma(I)$] = 0.040. $wR = 0.089$ (all 3346 reflections).
- 3**: $\text{C}_{16}\text{H}_{13}\text{N}_8\text{S}_4$, MW = 445.56, triclinic, space group $P-1$, $a = 7.0280(10)$, $b = 9.6690(10)$, $c = 15.000(2) \text{ \AA}$, $\alpha = 86.46$, $\beta = 81.150(10)$, $\gamma = 79.990(10)^\circ$, $V = 991.2(2) \text{ \AA}^3$, $Z = 2$, $T = 293(2)$, $\rho(\text{calcd}) = 1.490 \text{ g cm}^{-3}$,

$\mu = 0.500 \text{ mm}^{-1}$, $F(000) = 456$. The refinement converged to final R [for 1882 reflections with $I > 2\sigma(I)$] = 0.0607, $wR = 0.1788$ (all 3771).

- 3'**: $\text{C}_8\text{H}_6\text{N}_4\text{S}_2$, MW = 222.31, triclinic, space group $P\bar{1}$, $a = 7.0397(7)$, $b = 9.6707(9)$, $c = 15.0053(16) \text{ \AA}$, $\alpha = 86.432(8)$, $\beta = 81.153(8)$, $\gamma = 79.992(8)^\circ$, $V = 993.37(17) \text{ \AA}^3$, $Z = 4$, $T = 295(2)$, $\rho(\text{calcd}) = 1.49 \text{ g cm}^{-3}$, $\mu = 0.509 \text{ mm}^{-1}$, $F(000) = 456$. The refinement converged to final R [for 2267 reflections with $I > 2\sigma(I)$] = 0.038, $wR = 0.093$ (all 3490 reflections).
- 4**: $\text{C}_{21}\text{H}_{15}\text{I}_2\text{N}_3\text{S}_6$, MW = 755.52, triclinic, space group $P\bar{1}$, $a = 9.927(1)$, $b = 10.808(3)$, $c = 12.335(1) \text{ \AA}$, $\alpha = 88.54(2)$, $\beta = 75.30(1)$, $\gamma = 85.60(1)^\circ$, $V = 1276.3(4) \text{ \AA}^3$, $Z = 2$, $T = 223(2)$, $\rho(\text{calcd}) = 1.966 \text{ g cm}^{-3}$, $\mu = 2.971 \text{ mm}^{-1}$, $F(000) = 728$. The refinement converged to final R [for 3307 reflections with $I > 2\sigma(I)$] = 0.046, $wR = 0.161$ (all 4478 data).
- 5**: $\text{C}_7\text{H}_5\text{N}_3\text{O}_2\text{S}\cdot\text{H}_2\text{O}$, MW = 21320, monoclinic, space group $P2_1/c$, $a = 3.8349(6)$, $b = 21.788(3)$, $c = 10.2527(15) \text{ \AA}$, $\beta = 95.922(14)^\circ$, $V = 852.1(2) \text{ \AA}^3$, $Z = 4$, $\rho = 1.58 \text{ g cm}^{-3}$, $\mu = 0.35 \text{ mm}^{-1}$, $F(000) = 446$. The refinement converged to final R [for 877 reflections with $I > 2\sigma(I)$] = 0.108, $wR = 0.270$ (all 1553 data).
- 6a-6b**: $0.73\text{C}_7\text{H}_5\text{N}_3\text{O}_3\cdot 0.27\text{C}_7\text{H}_5\text{N}_3\text{O}_2\text{S}\cdot 1.73\text{H}_2\text{O}$, MW = 214.63, monoclinic, space group $P2_1/c$, $a = 3.659(1)$, $b = 9.871(1)$, $c = 25.156(5) \text{ \AA}$, $\beta = 90.15(3)^\circ$, $V = 908.6(5) \text{ \AA}^3$, $Z = 4$, $\rho = 1.56 \text{ g cm}^{-3}$, $\mu = 1.69 \text{ mm}^{-1}$, $F(000) = 444$. The refinement converged to final R [for 976 reflections with $I > 2\sigma(I)$] = 0.112, $wR = 0.254$ (all 1157 data).

Crystallographic data (excluding structure factors) for the structural analysis have been deposited with the Cambridge Crystallographic Data Centre No. CCDC-850425 (**1**), 850427 (**2**), 850841 (**3**), 850426 (**3'**), 849060 (**4**), 850428 (**5**), and CCDC 850427 (**6a-6b**). Copies of this information may be obtained free of charge from The Director, CCDC, 12 Union Road, Cambridge, CB2 1EZ, UK. Fax: +44(1223)336-033, e-mail: deposit@ccdc.cam.ac.uk, or www: www.ccdc.cam.ac.uk.

Computational Details

All geometrical optimizations and energy calculations were carried out using the DMol3 algorithm

[61]. The generalized gradient corrections to the local density approximation were employed via the BLYP functional. DND (double numerical with d polarization) basis set, which is comparable to the 6-31G* basis set, was used.

Electrochemistry Studies

CVA measurements were carried out in CH_2Cl_2 and DMF solutions with 0.15 M Bu_4NBF_4 as supporting electrolyte using potentiostat a IPC model compact in a conventional and one-compartment three-electrode cell (10 mL of solution). A platinum (Pt) disk electrode with an active surface area of 0.125 cm^2 was used as the working electrode. The electrode was thoroughly polished and rinsed before measurements. A platinum counterelectrode and standard Ag/AgCl/KCl(aq. reference electrode (RE) were applied. The differential pulse voltammograms were recorded using the same equipment under the same conditions. All CVA experiments were performed at a scan rate of 200 mV/s. The solutions were thoroughly deaerated by passing Ar through the solutions prior to the CV experiments. The experiments were carried out in Ar atmosphere as well.

ACKNOWLEDGMENT

This work was carried out in partial fulfillment of the requirements for Ph.D. theses of GJC (**1,3',4,5**, and **5a-5b**) and CDA (**2,3**) under the supervision of SKH within the framework of the graduate program in Bioinorganic Chemistry coordinated by NHS, KH, NH, and ERM acknowledge a NATO grant for the exchange of scientists (PDD(CP)-(CBP.NR.NRCLG 983167). The Ministry of Higher Education (Malaysia) is thanked for funding crystal-engineering studies through the High-Impact Research scheme (UM.C/HIR/MOHE/SC/12).

REFERENCES

- [1] Daga, V.; Hadjikakou, S. K.; Hadjiliadis, N.; Kubicki, M.; dos Santos, J. H. Z.; Butler, I. S. *Eur J Inorg Chem* 2002, 1718–1728.
- [2] Antoniadis, C. D.; Corban, G.; Hadjikakou, S. K.; Hadjiliadis, N.; Kubicki, M.; Warner, S.; Butler, I. S. *Eur J Inorg Chem* 2003, 1635–1640.
- [3] Antoniadis, C. D.; Hadjikakou, S. K.; Hadjiliadis, N.; Kubicki, M.; Butler, I. S. *Eur J Inorg Chem* 2004, 4324–4329.
- [4] Antoniadis, C. D.; Hadjikakou, S. K.; Hadjiliadis, N.; Kubicki, M.; Butler, I. S. *New J Chem* 2005, 29, 714–720.
- [5] Corban, G. J.; Hadjikakou, S. K.; Hadjiliadis, N.; Kubicki, M.; Tiekink, E. R. T.; Butler, I. S.; Drougas, E.; Kosmas, A. M. *Inorg Chem* 2005, 44, 8617–8627.

- [6] Antoniadis, C. D.; Hadjikakou, S. K.; Hadjiliadis, N.; Papakyriakou, A.; Baril, M.; Butler, I. S. *Chem Eur J* 2006, 12, 6888–6897.
- [7] Hadjikakou, S. K.; Hadjiliadis, N. *Bioinorg Chem Appl* 2006, Article ID 60291, pp. 1–10.
- [8] dos Santos, J. H. Z.; Butler, I. S.; Daga, V.; Hadjikakou, S. K.; Hadjiliadis, N. *Spectrochim Acta A* 2002, 58, 2725–2735.
- [9] Parigoridi, I.-E.; Corban, G. J.; Hadjikakou, S. K.; Hadjiliadis, N.; Kourkoumelis, N.; Kostakis, G.; Psycharis, V.; Raptopoulou, C. P.; Kubicki, M. *Dalton Trans* 2008, 5159–5165.
- [10] Taurog, A. In *Endocrinology*; DeGroot, L., Ed.; Academic Press: London, 1979; Vol. 1, p. 331.
- [11] Morris, D. R.; Hager, L. P. *J Biol Chem* 1966, 241, 3582–3589.
- [12] Nakataka, A.; Hidaka, H. *J Clin Endocrinol Metab* 1976, 43, 152–158.
- [13] Martidale. In *The Extra Pharmacopoeia*; 28th ed.; J. E. F. Reynolds, Ed.; The Pharmaceutical Press: London, 1982.
- [14] Esseffar, M.; Bouab, W.; Lamsabhi, A.; Abboud, J. L. M.; Notario, R.; Yanez, M. *J Am Chem Soc* 2000, 122, 2300–2308.
- [15] Bigoli, F.; Deplano, P.; Ienco, A.; Mealli, C.; Mercuri, M. L.; Pellinghelli, M. A.; Pintus, G.; Saba, G.; Trogu, E. F. *Inorg Chem* 1999, 38, 4626–4636.
- [16] Bigoli, F.; Deplano, P.; Mercuri, M. L.; Pellinghelli, M. A.; Sabatini, A.; Trogu, E. F.; Vacca, A. *J Chem Soc, Dalton Trans* 1996, 3583–3598.
- [17] Freeman, F.; Ziller, J. W.; Po, H. N.; Keindl, M. C. *J Am Chem Soc* 1988, 110, 2586–2591.
- [18] Arzei, D.; Deplano, P.; Trogu, E. F.; Bigou, F.; Pellinghelli, M. A.; Vacca, A. *Can J Chem* 1988, 66, 1483–1489.
- [19] Cristiani, F.; Devillanova, F. A.; Diaz, A.; Verani, G. *J Chem Soc, Perkin Trans* 1984, 2, 1383–1386.
- [20] Devillanova, F. A.; Verani, G. *Tetrahedron* 1979, 35, 511–514.
- [21] Aragoni, M. C.; Arca, M.; Demartin, F.; Devillanova, F. A.; Garau, A.; Isaia, F.; Lippolis, V.; Verani, G. *J Am Chem Soc* 2002, 124, 4538–4539.
- [22] Boyle, P. D.; Godfrey, S. M. *Coord Chem Rev* 2001, 223, 265–299.
- [23] Deplano, P.; Ferraro, J. R.; Mercuri, M. L.; Trogu, E. F. *Coord Chem Rev* 1999, 188, 71–95.
- [24] Svensson, P. H.; Kloo, L. *Chem Rev* 2003, 103, 1649–1684.
- [25] Deplano, P.; Devillanova, F. A.; Ferraro, J. R.; Isaia, F.; Lippolis, V.; Mercuri, M. L. *Appl Spectrosc* 1992, 46, 1625–1629.
- [26] du Mont, W. W.; Muges, G.; Wismach, C.; Jones, P. G. *Angew Chem, Int Ed* 2001, 40, 2486–2489.
- [27] Pennington, W. T.; Hanks, T. W.; Arman, H. D. *Struct Bonding* 2008, 126, 65–104.
- [28] Ouvrard, C.; Le, J.-Y.; Questel Berthelot, M.; Laurence, C. *Acta Crystallogr, Sect B: Struct Sci* 2003, 59, 512–526.
- [29] O'Brien; P. *J Chem-Biochem Interact* 2000, 129, 113–139.
- [30] Rawitch, A. B.; Taurog, A.; Chernoff, S. B.; Dorris, M. L. *Arch Biochem Biophys* 1979, 194, 244–257.
- [31] Magnusson, R. P.; Taurog, A.; Dorris, M. L. *J Biol Chem* 1984, 259, 197–205.
- [32] Magnusson, R. P.; Taurog, A.; Dorris, M. L. *J Biol Chem* 1984, 259, 13783–13790.
- [33] Huwiler, M.; Burgi, U. Kohler, H. *Eur J Biochem* 1985, 147, 469–476.
- [34] Johnson, T. B.; Edens, C. O. *J Am Chem Soc* 1942, 64, 2706–2708.
- [35] Herbstein, F. H.; Schwotzert, W. *J Am Chem Soc* 1984, 106, 2367–2373.
- [36] Humphrey, S. M.; Wood, P. T. *Acta Crystallogr, Sect E: Struct Rep Online* 2003 59, o1364.
- [37] Bi, W.; Sun, D.; Cao, R.; Hong, M. *Acta Crystallogr, Sect E: Struct Rep Online* 2002, 58, o837.
- [38] Kresinski, R. A.; Fackler, J. P., Jr. *Acta Crystallogr Sect C Cryst Struct Commun* 1994 50, 2039.
- [39] Zhu, J.; Zhao, Y.; Hong, M.; Sun, D.; Shi, Q.; Cao, R. *Chem Lett* 2002, 484.
- [40] Furberg, S.; Solbakk, J. *Acta Chem Scand* 1973, 27, 2536.
- [41] Jensen, G. B.; Smith, G.; Sagatys, D. S.; Healy, P. C.; White, J. M. *Acta Crystallogr, Sect E: Struct Rep Online* 2004, 60, o2438.
- [42] Simmons, C. J.; Lundeen, M.; Seff, K. *Inorg Chem* 1979, 18, 3444.
- [43] Batsanov, S. S. *Inorg Mater* 2001, 37, 871–885.
- [44] Radha, A. *Z Kristallogr* 1985. 171, 225.
- [45] Zhang, R.-F.; Qiu, L.-L.; Li, F.; Ma, C.-L. *Chin J Chem* 2004, 22, 768.
- [46] Van Bolhuis, F.; Koster, P. B.; Migchelsen, T. *Acta Crystallogr* 1967, 23, 90.
- [47] Pauling, L. *The Nature of the Chemical Bond*, 3rd ed.; Cornell University Press: Ithaca, NY, 1960.
- [48] Bigoli, F.; Deplano, P.; Mercuri, M. L.; Pellinghelli, M. A.; Sabatini, A.; Trogu, E. F.; Vacca, A. *J Chem Soc, Dalton Trans* 1996, 3583.
- [49] Bigoli, F.; Deplano, P.; Ienco, A.; Mealli, C.; Mercuri, M. L.; Pellinghelli, M. A.; Pintus, G.; Saba, G.; Trogu, E. F. *Inorg Chem* 1999, 38, 4626.
- [50] Zanello, P. *Inorganic Electrochemistry* Cambridge 2003, 579.
- [51] Mann, Ch. Barnes K. *Electrochemical Reactions in Nonaqueous Systems*; Marcel Dekker: New York, 1970.
- [52] Beizer, M.; Lund, H. (Eds.). *Organic Electrochemistry*; Marcel Dekker: New York, 1983.
- [53] Izutsu, K. *Electrochemistry in Nonaqueous Solutions*; Wiley-VCH: Weinheim, Germany, 2002.
- [54] Grimshaw, G. *Electrochemical Reactions and Mechanisms in Organic Chemistry*; Elsevier: Amsterdam, the Netherlands, 2000.
- [55] Magdesieva, T. V.; Butin, K. P. *Russ Chem Rev* 1993, 62, 359–385.
- [56] Chambers, J. Q.; Moses, P. R.; Shelton, R. N.; Coffen, D. L. *J Electroanal Chem* 1972, 38, 245.
- [57] Agilent Technologies. *CrystAlisPro* (Version 171.35.4), 2010.
- [58] Blessing, R. H. *J Appl Crystallogr* 1989; 22, 396–397.
- [59] Sheldrick, G. M. *Acta Crystalslogr, Sect A* 2008; 64, 112.
- [60] Sheldrick, G. M. *SADABS*; Bruker AXS Inc.; Madison, WI, 2007.
- [61] (a) Delley, B. *J Chem Phys* 1990, 92, 508; (b) Delley, B. *J Chem Phys* 2000, 113, 7756.